Thermoelectric Properties of Y_2CX_2 (X= F, Cl, Br, I and O) Monolayers: A First-Principles Boltzmann Transport Study

Shirin Amirian[1], Negin Fatahi[1]*, Mosayeb Naseri[2], Borhan Arghavani Nia[1]

1.Department of Physics, Ker.C., Islamic Azad University, Kermanshah, Iran
2.Department of Chemistry, Department of Physics and Astronomy, CMS – Center for Molecular Simulation, IQST – Institute for Quantum Science and Technology, Quantum Alberta, University of Calgary, 2500 University Drive NW, Calgary, Alberta, Canada, T2N 1N4

Email addresses: n60.fatahi@iau.ac.ir

Abstract

In this research, the thermoelectric properties of two-dimensional Y_2CX_2 (X = F, Cl, Br, I, and O) structures have been investigated using semi-classical Boltzmann theory within the constant relaxation time approximation (CRTA) framework. These structures have been previously validated for structural, thermodynamic, dynamic, and mechanical stability, and their electronic, optical, and photovoltaic properties have been reported. In this study, key thermoelectric parameters were calculated and analyzed in the temperature range of 0 to 1000 K. Based on the obtained results, Y_2CCl_2 and Y_2CF_2 structures exhibit the highest thermoelectric performance with ZT values of approximately 0.578 and 0.410 at 300 K, respectively, demonstrating competitive performance compared to well-known materials such as MoS_2 (0.11), $Ti_3C_2T_x$ (0.22), and Bi_2Te_3 (0.80). The comprehensive analysis of these results highlights the high potential of the Y_2CX_2 family of MXenes for converting thermal energy into electricity, particularly at high temperatures.

Keywords: Thermoelectric properties, MXenes, Seebeck coefficient, Power factor, Figure of merit, Boltzmann transport theory

1. Introduction

Rising global energy requirement and the urgent need to reduce reliance on nonrenewable resources have stimulated interest in thermoelectric technologies capable of directly converting heat into electricity [1]. The performance of thermoelectric materials is characterized by the dimensionless figure of merit (ZT), which depends on the Seebeck coefficient (S), electrical conductivity (σ) and total thermal conductivity (κ). Simultaneous optimization of these interdependent quantities remains an important challenge for achieving high-efficiency thermoelectric [2].

In recent years, two-dimensional materials have offered new prospects for enhancing thermoelectric performance owing to their unique properties [3]. In particular, MXenes with the general formula $M_{n+1}X_nT_x$ have attracted considerable attention due to their structural stability, high electrical conductivity and surface engineering tunability [4].

Theoretical and experimental studies have demonstrated that modifying the surface functional groups of MXenes with –O, –F, –OH and –Cl can significantly alter their thermoelectric properties. For instance, Sarikurt et al. reported that Ti_2CO_2 and Zr_2CO_2 MXenes can achieve a figure of merit of up to ZT≈ 1.1 in the presence of appropriate surface groups [5]. Furthermore, Karmakar and Saha Dasgupta, based on theoretical calculations, predicted that bimetallic MXenes such as Ti–Mo–C_2F_2 could reach a ZT value of approximately 3.1 at around 800 K [6]. In addition, Bandaru et al. conducted a comprehensive review outlining the prospects and challenges of MXene materials for thermoelectric applications [7].

The specific family Y_2CX_2 (X= F, Cl, Br, I and O) represents an emerging class of MXenes. In our previous work, we investigated the structural, dynamical and mechanical stability of these monolayers [8]. In the present study, by systematically evaluating the thermoelectric properties of all five terminations using semiclassical Boltzmann transport theory within the constant relaxation time approximation (CRTA) over a broad temperature range (0–1000 K) complements that investigation. Finally, we compare the computed transport coefficients with representative 2D thermoelectric materials to highlight the potential

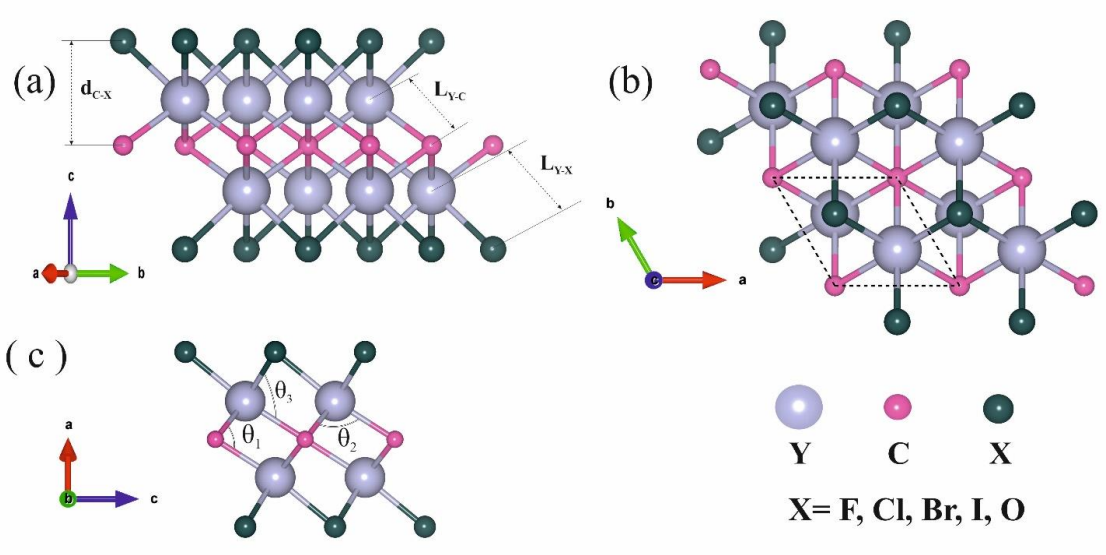

Figure 1: Top and side views of the atomic geometric configurations of monolayer Y_2CX_2 (X= F, Cl, Br, I and O).

advantages and limitations of Y_2CX_2 monolayers.

2. Computational Methodology

In our earlier publication [8], we performed first-principles calculations on the Y_2CX_2 (X= F, Cl, Br, I and O) MXene family to investigate their structural stability, phonon and mechanical properties, as well as their electronic, optical and photovoltaic behaviors. To avoid redundancy, only a brief overview is provided here and the atomic configuration of Y_2CO_2 (which was not included previously) is illustrated in Figure 1.
The phonon spectrum and electronic band structure, along with the total density of states (TDOS) of the monolayer metallic Y_2CO_2 in its ground state calculated using the PBE, mBJ and HSE06 approaches as well as the table of structural parameters and elastic constants, together with the angular dependence plots of Young's modulus and Poisson's ratio for the two-dimensional Y_2CX_2 (X= F, Cl, Br, I and O) nanostructures, are included in the Supplementary Information (Figures S1 and S2 and Tables S1 and S2).

In this manuscript, we extend our previous work by calculating and analyzing the thermoelectric performance of these previously verified stable monolayers. The computational setup, including the exchange–correlation functional, plane-wave cutoff energy and k-point sampling, is identical to that used in Ref. [8], ensuring consistency between the two studies.
The thermoelectric transport coefficients were computed using the BoltzTraP2 code [10], which interpolates the electronic band energies and solves the semiclassical Boltzmann transport equations within the constant relaxation time approximation (CRTA). Although related theoretical investigations on Y_2C-based MXenes have been reported [8, 9], the thermoelectric behavior of the fully terminated Y_2CX_2 monolayers is explored here for the first time.
Within this framework, we evaluated the Seebeck coefficient (S), electrical conductivity (σ/τ), electronic thermal conductivity scaled by relaxation time (κ_e/τ) and derived quantities such as the power factor (σS^2) and the thermoelectric figure of merit (ZT). All calculations were performed for temperatures ranging from 0 to 1000 K and for chemical potentials around the Fermi level to probe the intrinsic transport behavior.
The thermoelectric transport coefficients were calculated using semiclassical Boltzmann transport theory within the constant relaxation time approximation (CRTA), as implemented in the BoltzTraP2 code [10]. In this framework, the electrical conductivity tensor $\sigma_{\alpha\beta}$, Seebeck coefficient $S_{\alpha\beta}$ and electronic thermal conductivity $\kappa^{el}_{\alpha\beta}$ are expressed as follows:

$$\sigma_{\alpha\beta}(\varepsilon) = \frac{e^2}{N}\sum_{i,k} \tau v_\alpha(i,j)\frac{\delta(\varepsilon-\varepsilon_{i,k})}{d\varepsilon} \quad (1)$$

$$\sigma_{\alpha\beta}(T,\mu) = \frac{1}{\Omega}\int \sigma_{\alpha\beta}(\varepsilon)[-\frac{\partial f_0(T,\varepsilon,\mu)}{\partial\varepsilon}]\,\partial\varepsilon \quad (2)$$

$$S_{\alpha\beta}(T,\mu) = \frac{1}{eT\sigma_{\alpha\beta}\Omega}\int \sigma_{\alpha\beta}(\varepsilon-\mu)[-\frac{\partial f_0(T,\varepsilon,\mu)}{\partial\varepsilon}]\,\partial\varepsilon \quad (3)$$

$$\kappa^{el}_{\alpha\beta}(T,\mu) = \frac{1}{\Omega}\int \sigma_{\alpha\beta}(\varepsilon-\mu)^2[-\frac{\partial f_0(T,\varepsilon,\mu)}{\partial\varepsilon}]\,\partial\varepsilon \quad (4)$$

where e is the elementary charge, N is the number of k-points sampled in the Brillouin zone, τ is the relaxation time and υα and υβ are the group velocities of the charge carriers along the α and β directions, respectively. ε (i.k) denotes the electronic energy of band i at wave vector k, μ is the chemical potential, Ω is the unit-cell volume and f0 (T.ε.μ) is the Fermi–Dirac distribution function. These equations form the basis for evaluating the Seebeck coefficient, electrical conductivity and electronic thermal conductivity as functions of temperature and chemical potential3**.**

Results and Discussion

The Seebeck coefficient (S), σ/τ, κ_e/τ, $\sigma S^2/\tau$ and ZT using the approximations detailed in [11-13] calculated for the five Y_2CX_2 monolayers at 300 K and are summarized in Table 1. Notably, Y_2CCl_2 has the largest positive Seebeck coefficient and the highest ZT at this temperature. The Seebeck coefficient (S) is defined as the ratio between the induced thermoelectric voltage and the temperature difference across the material, as given by Eq**.** (5):

$$S = -\frac{\Delta V}{\Delta T} \quad (5)$$

Table 1: Calculated thermoelectric parameters of Y_2CX_2 MXenes (X= F, Cl, Br, I and O) at 300 K.

System	S (μV/K)	$\sigma/\tau_0 (10^{15} \frac{1}{\Omega, m, s})$	κ_e/τ_0 (10^{10} W/m.K.s)	$\sigma S^2/\tau_0$ (10^8 W/m.K^2. s)	ZT
Y_2CF_2	131	3751	4690	641	0.410
Y_2CCl_2	213	3259	7660	1474	0.578
Y_2CBr_2	-9.71	264100	255780	249	0.003
Y_2CI_2	17.2	44560	26910	131	0.015
Y_2CO_2	10.2	82730	63660	86	0.004

The Seebeck coefficient is highly sensitive to carrier type and concentration. Positive S indicates hole-dominated (p-type) transport, whereas negative S indicates electron-dominated (n-type) transport [14-16] . In our results, Y_2CCl_2 and Y_2CF_2 structures have large positive Seebeck coefficients (213 μV/K and 131 μV/K, respectively), while Y_2CBr_2 structure has a small negative S (~ –9.7 μV/K), consistent with its metallic or degenerate nature at the Fermi level. For Y_2CF_2 structure, the S is larger at low temperatures and decreases by increasing temperature, which is characteristic of semiconductors and attributable to increased intrinsic carrier concentrations and smearing of the Fermi–Dirac distribution at elevated T [17-19].

The total thermal conductivity (κ_{total}) of a material arises from two fundamental contributions: the electronic component (κ_e) and the lattice or phonon component (κ_l). Given the low-dimensional nature of these systems, we considered a conservative, estimated value for (κ_l) from recent experimental and theoretical reports on similar MXenes to calculate a realistic and reliable value for ZT. This ensures that our reported thermoelectric efficiency is not overvalued and remains within a physically plausible range.The overall heat transport can therefore be expressed as**:**

$$\kappa_{total} = \kappa_e + \kappa_l \quad (6)$$

The electronic term (κ_e) originates from the movement of charge carriers (electrons and holes), while the lattice term (κ_l) represents heat carried by lattice vibrations (phonons) [20 ,21]. In metallic and semimetallic systems, where electronic conduction dominates, κ_e often constitutes a significant portion of the total thermal conductivity**.**

Within the Wiedemann–Franz law, the electronic thermal conductivity is approximately proportional to the electrical conductivity (σ) and the absolute temperature (T), as described by**:**

$$\kappa_e = L\sigma T \quad (7)$$

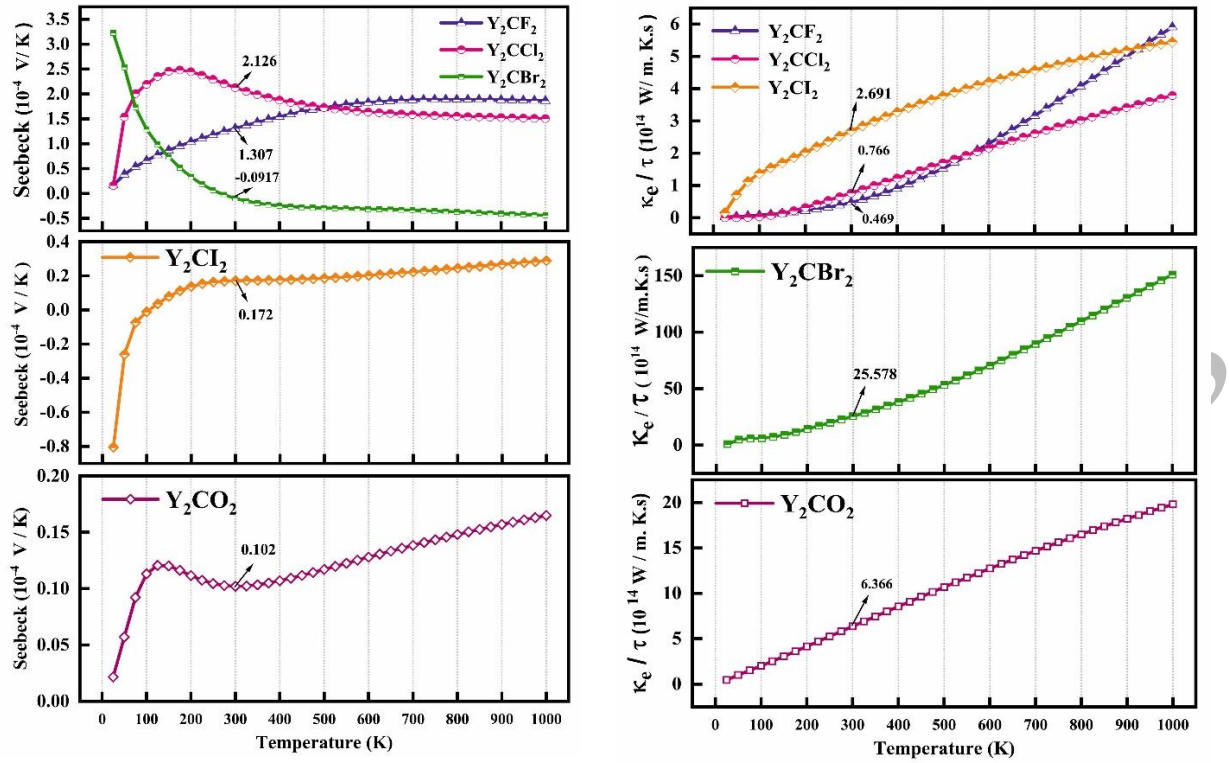

Figure 2: Calculated Seebeck coefficient and thermal conductivity of Y_2CX_2 monolayers (X= F, Cl, Br, I and O) as a function of temperature.

where L is the Lorenz number, which takes the theoretical value of (≈ 2.44×10^{-8} WΩ/K²) for ideal free-electron systems [21, 22]. This relation assumes a parabolic electronic band structure and energy-independent scattering time. However, for low-dimensional materials such as 2D MXenes, these assumptions may not be strictly valid. Consequently, the Lorenz number can deviate from its classical value, depending on the degree of band non-parabolicity, carrier concentration and temperature .

The electronic contribution to thermal conductivity (κ_e) arises from charge carriers and is a component of the total thermal conductivity [20,21].

In our results, the Y_2CBr_2 structure has the largest κ_e (limiting its ZT), while Y_2CCl_2 and Y_2CF_2 have comparatively lower κ_e, which has higher thermoelectric efficiency [23, 24]. The electrical conductivity within the Boltzmann transport formalism is expressed as:

$$\sigma = e^2 \int \tau(\varepsilon) v^2(\varepsilon) D(\varepsilon) \left(-\frac{f \partial}{\varepsilon \partial} \right) d\varepsilon \quad (8)$$

Also, the electrical conductivity (reported as σ/τ) was computed within the Boltzmann formalism. The high σ often leads to reduced S, so an optimal balance between σ and S is necessary for maximizing the power factor (σS^2) and ZT [25–30]. The power factor, which evaluates the combined effect of electrical conductivity and Seebeck coefficient, is defined as :

$$PF = \sigma S^2 \quad (9)$$

The Y_2CBr_2 structure exhibits very high σ/τ but its S is low, which yields a small $\sigma S^2/\tau$ (and thus small PF). Among all studied systems, Y_2CCl_2 and Y_2CF_2 exhibit the most favorable balance between electrical conductivity and Seebeck coefficient, leading to the highest values of $\sigma S^2/\tau$ and power factor (PF) throughout the investigated temperature range (0–1000 K).

Figure 2 shows the temperature dependence of S and κ_e for all five monolayers; Figure 3 presents σ and σS^2 (power factor) as functions of temperature, while Figure 4 displays ZT for proposed monolayers [31–37]. The dimensionless thermoelectric figure of merit is given by:

$$ZT = \frac{\sigma S^2 T}{\kappa} \quad (10)$$

The dimensionless figure of merit (ZT) is defined as $ZT = \sigma S^2 T/(\kappa_e+\kappa_l)$, where S, σ, κ_e and κ_l are the Seebeck coefficient, electrical conductivity, electronic thermal conductivity and lattice thermal conductivity, respectively.

The calculated ZT values reveal that Y_2CCl_2 (≈ 0.578 at 300 K) and Y_2CF_2 (≈ 0.410) possess superior thermoelectric performance compared to other representative 2D materials such as MoS_2 (ZT≈ 0.11) and Ti_3C_2 (ZT≈ 0.22). This improvement can be attributed to the more favorable electronic transport characteristics and optimized balance between σ and S in the Y_2CX_2 family, although their ZT values remain below those of conventional bulk thermoelectrics like Bi_2Te_3 (ZT≈ 0.80) [38-45].

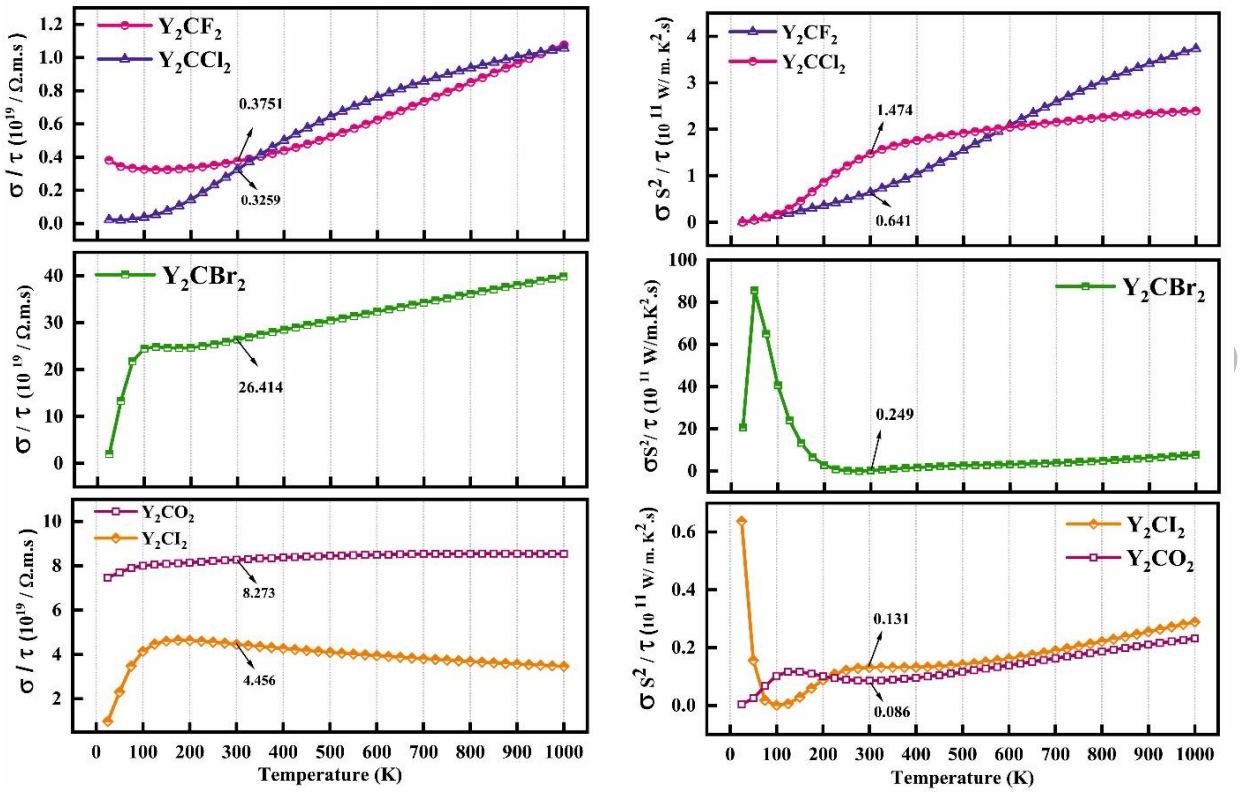

Figure 3: Calculated electrical conductivity and power factor of Y_2CX_2 monolayers (X= F, Cl, Br, I and O) as a function of temperature.

Our analysis indicates that termination plays a dominant role. The lighter halogen terminations (F, Cl) improve the thermoelectric performance relative to terminations (Br, I) or oxygen. These trends can be explained by variations in electronegativity and atomic radius, which together influence the electronic band structure and phonon scattering mechanisms.

The superior power factor (PF) in Y_2CCl_2 and Y_2CF_2 compared to other members of the family can be attributed to the significant modification of the electronic band structure by the surface termination elements (F First, the high electronegativity of F and Cl .and Cl) atoms leads to a strong orbital hybridization with the d-orbitals of Yttrium (Y), which effectively tunes the density of states (DOS) near the Fermi level. Specifically, these terminations introduce a 'pudding-mold' type band structure or flat-dispersive bands, which are known to enhance the Seebeck coefficient while maintaining relatively high electrical conductivity.

Second, regarding the scattering mechanisms, the different ionic radii and electronegativities of the functional groups modify the crystal potential. In the case of Y_2CCl_2, the larger atomic radius of Cl compared to F results in a slight expansion of the lattice, which in certain reduces the electronic effective mass (m) crystallographic directions. This reduction in (m*) enhances carrier mobility (μ) and subsequently the electrical conductivity (σ/τ). Furthermore, the surface terminations act as a chemical pressure that modulates the band gap and the curvature of the valence/conduction bands. The synergy between a high Seebeck coefficient (due to band flattening) and improved conductivity (due to optimized effective mass) results in the observed high-power factor in these two specific structures [45].

Overall, these findings suggest that surface engineering (through appropriate terminal element selection) provides an effective route to tune the thermoelectric performance of Y_2C-based MXenes. Strategies such as doping, strain engineering or heterostructure design could further enhance the power factor and reduce the lattice thermal conductivity, thereby improving ZT in future studies

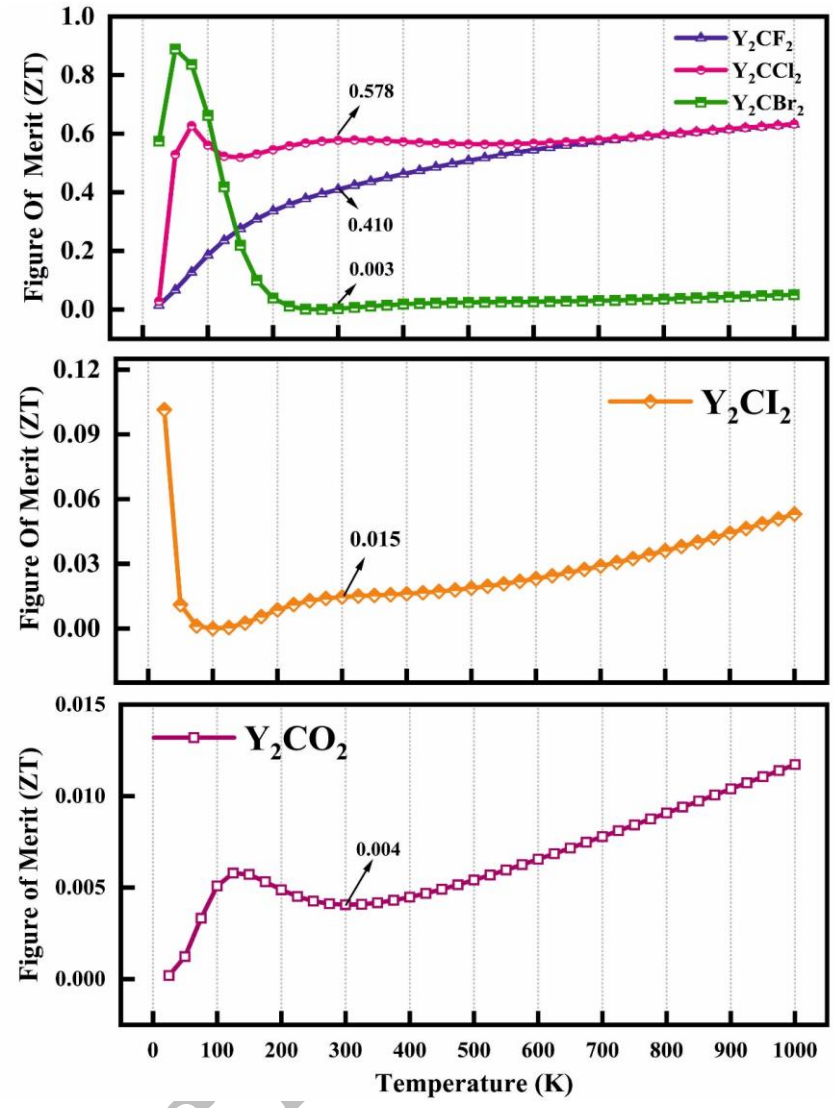

Figure 4: Calculated thermoelectric figure of merit (ZT) of Y_2CX_2 monolayers (X= F, Cl, Br, I and O) as a function of temperature

4. Conclusion

In this study, the thermoelectric properties of the two-dimensional semiconducting Y_2CX_2 (X= F, Cl, Br, I and O) were investigated using first-principles calculations. The results indicate that Y_2CCl_2 and Y_2CF_2 exhibit significant thermoelectric performance due to their relatively high Seebeck coefficients, favorable electrical conductivity and low lattice thermal conductivity. Among the studied structures, Y_2CCl_2 achieves the best performance with a figure of merit of ZT≈ 0.578 at 300 K. Moreover, the appreciable performance of Y_2CF_2 highlights the high potential of this structure for high-temperature thermoelectric applications. In contrast, Y_2CBr_2, Y_2CI_2 and Y_2CO_2 demonstrate lower efficiencies, which can be attributed to differences in the chemical and structural characteristics of the terminal element.

The comparison of these five structures indicates that the type of terminal element in MXene significantly influences their thermoelectric properties. Structures with lighter halogen elements such as F and Cl demonstrate superior performance compared to those containing heavier halogens like Br, I or O. These differences can be attributed to factors including variations in electronegativity, atomic size and their impact on the electronic and phononic band structures.

Overall, the results of this study suggest that terminal surface engineering in MXene structures, including the choice of an appropriate element, can play a crucial role in optimizing their thermoelectric performance. Future investigations may focus on further enhancing these properties through strategies such as doping, lattice strain engineering or heterostructure design to achieve even higher performance.

References

1) J Tang, R Zhu, Y H Pai, Z Zhao, C Xu and Z Liang, *Nano-Micro Lett* **17** (2024) 11.
2) G J Snyder and E S Toberer, *Nat Mater* **7** (2008)105–114.
3) H Zhou, Y Cai, G Zhang and Y Zhang, *npj Quantum Mater* **2** (2017) 18.
4) M Naguib, M Kurtoglu, V Presser, J Lu, J Niu, M Heon, L Hultman, Y Gogotsi and M W Barsoum, *Adv Mater* **23** (2011) 4248–4253.
5) S Sarikurt, D Çakır, M Keçeli and C Sevik, *Nanoscale* **10** (2018) 8859–8869.
6) S Karmakar and T S Dasgupta, *Phys Rev Mater* **4** (2020) 124007.
7) S Bandaru, A M Jastrzębska, M Birowska, *Appl Mater Today* **34** (2023) 101902.
8) S Amirian, N Fatahi and M Naseri, *Mater Today Commun* **42** (2025)111217.
9) N Modi, Y Naik, P H Jariwala, D B Shah and P B Thakor, *Solid State Commun* **372** (2023)115303.
10) G K H Madsen, J Carrete and M J Verstraete, *Comput Phys Commun* **231** (2018)140-145.
11) M Markov, S E Rezaei, S N Sadeghi, K Esfarjani and M Zebarjadi, *Phys Rev Mater* **3** (2019)095401.
12) K Behnia, *C R Phys* **23** (2022) 25-40.
13) G Prunet, F Pawula, G Fleury, E Cloutet, A J Robinson, G Hadziioannou and A Pakdel, *Mater Today Phys* **18** (2021)100402.
14) L Xi, J Yang, L Wu, J Yang and W Zhang, *J Materiomics* **2** (2016) 114-130.
15) B Zhu, M Liu, X Dong, J Li, P F Liu, X Chen, Z Liu, Y Zhang, F Gue and J Sui, *Natl Sci Rev* **12** (2025) nwae384.
16) D Byeon, R Sobota, K Hirata, S Singh, S Choi, M Adachi, Y Yamamoto, M Matsunami and T. Takeuchi, *J Alloys Compd* **826** (2020) 154155.
17) J Boy, M Handwerg, R Ahrling, R Mitdank, G Wagner and Z Galazka, *APL Mater* **7** (2019) 022526.
18) S UI Rehman, S Manickam and N F Firdous, *AIP Conf Proc* **2760** (2023) 020020.
19) B Xu and M J Verstraete, *Phys Rev Lett* **112** (2014)196603.
20) S S air and N Singh, *Mater Today Nano* **29** (2025) 100561.
21) X Wang, J Maassen and M Lundstrom, *J Appl Phys* **123** (2018) 214304.
22) H Ye and C Zhou, *Acta Metall Sin* **38** (2025) 720–732.
23) H S Kim, Z M Gibbs, Y Tang, H Wang and J Snyder, *APL Mater* **3** (2015) 041506.
24) G Pizzi, D Volja, B Kozinsky, M Fornari and N Marzari, *Comput Phys Commun* **185** (2014) 422-429.
25) L Qiu, Y Ouyang and F Li, *Micro Nano Therm Transp* Pages (2022) 19-45.
26) N Jia, J Cao, X Y Tan, J Dong, H Liu, C K I Tan, J Xu, Q Yan, X J Loh and A Suwardi, *Mater Today Phys* **21** (2021) 100519.
27) R Kumar and B Muralidharan, *J Appl Phys* **137** (2025) 094301.
28) W Liu, H S Kim, Q Jie and Z Ren, *Scripta Mater* **111** (2016) 3-9.
29) R F Garmroudi, M Parzer, A Pustogow, T Mori and E Bauer, *Phys Rev Appl* **21** (2024) 014002.
30) A Dadhich, K Kumari, A K Patra, B Srinivasan, S Perumal, M S R Rao and K Sethupathi, *J Mater Chem A* **13** (2025) 16770-16784.
31) K S Bano, B Govind, A Bhardwaj, K Bhatt and D K Misra, *J Electron Mater* **50** (2021) 6037–6059.
32) M Naseri, D R Salahub, S Amirian and M A Rashid, *J Solid State Chem* **314** (2022) 123385.
33) Y Lobunets, *J Electron Mater* **48** (2019) 1896–1901.
34) M Naseri, S Amirian, M Faraji, M A Rashid, M P Lourenço, V Thangadurai and D R Salahub, *Phys Chem Chem Phys* **26** (2024) 946-957.
35) M Naseri, D R Salahub, S Amirian, H Shahmohamadi, M A Rashid, M Faraji and N Fatahi, *Mater Today Commun* **35** (2023) 105617.
36) Z Jin, Q Liao, H Fang, Z Liu, W Liu, Z Ding, T Luo and N Yang, *Sci Rep* **5** (2015) 18342.
37) D P Rai, T V Vu, A Laref, M A Hossain, E Haquee, S Ahmad, R Khenatag and R K Thapa, *RSC Adv* **10** (2020) 18830-18840.
38) A B Mohammad R, M Hayati and D A Ömer F, *Curr Nanosci* **17** (2021)423-446(24).
39) J Tang, R Zhu, Y H Pai, Y Zhao, C Xu and Z Liang, *Nano-Micro Lett* **17** (2025).
40) F Liu, Y H Wu, Q Zhang, T J Zhu and X B Zhao, *Rare Met* **40** (2021) 513–520.
41) D Teweldebrhan, V Goyal and A A Balandin, *Nano Lett* **10** (2010) 1209.
42) M Khisti, S Singh and R K Pandey, *Mater Today Commun* **25** (2020) 101431.
43) D Wickramaratne, F Zahid, R K Lake, *J Chem Phys* **140** (2014) 124710.
44) H Kim, S M Anand and S A Kim, *Nano Energy* **35** (2017) 312-318.
45) A D Satterthwaite and J P Heremans, *J Electron Mater **36*** (2007) 718-724.

Supplementary Files

Table S-1: Structural parameters of Y_2CX_2 (X = F, Cl, Br, I, O).

System	Y_2CF_2	Y_2CCl_2	Y_2CBr_2	Y_2CI_2	Y_2CO_2
a = b (Å)	3.60	3.71	3.78	3.88	3.54
C (Å)	15.49	22.25	22.63	23.25	15.49
$L_{Y\text{-}C}$ (Å)	2.49	2.54	2.55	2.59	2.70
$L_{Y\text{-}X}$ (Å)	2.37	2.77	2.91	3.11	2.18
$d_{C\text{-}X}$ (Å)	3.26	3.79	3.92	4.13	3.24
θ_1 (deg)	87.6	86.1	84.58	83.26	98.00
θ_2 (deg)	92.4	93.89	95.42	96.75	81.99
θ_3 (deg)	84.22	90.87	91.30	92.31	82.34

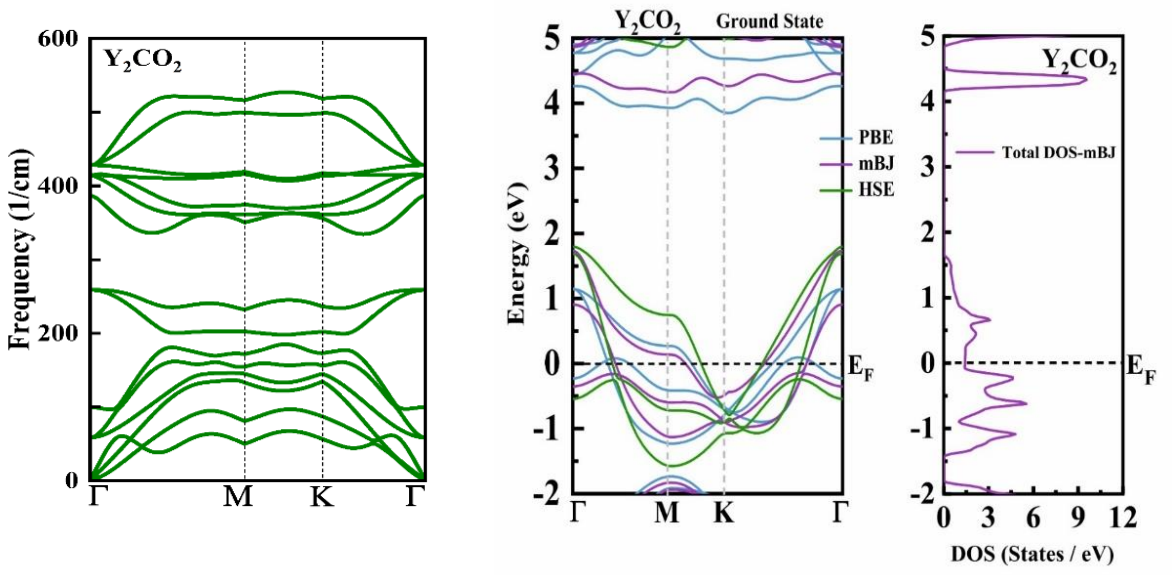

Figure S-1: Phonon spectrum and electronic band structure along with the total density of states (TDOS) using PBE, mBJ, and HSE06 approaches for the monolayer metallic Y_2CO_2 at the ground state.

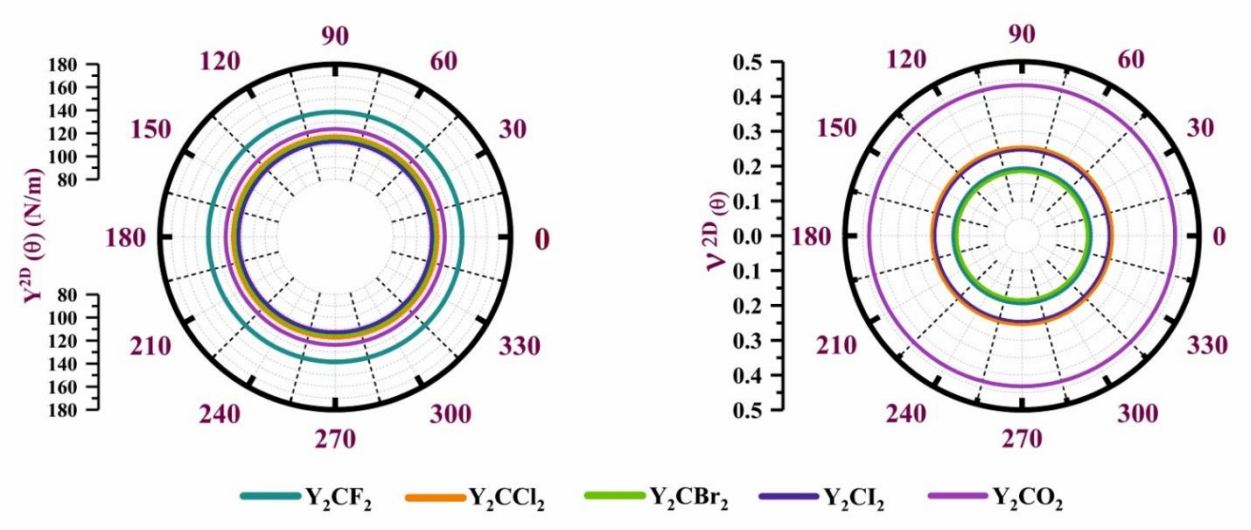

Figure S-2: Angular dependence of Young's modulus and Poisson's ratio for Y_2CX_2 monolayers (X = F, Cl, Br, I, O).

Table S-2: Elastic constants of two-dimensional Y_2CX_2 nanostructures (X = F, Cl, Br, I, O).

System	C_{11}(N/m)	C_{22}(N/m)	C_{12}(N/m)	G=C_{66}(N/m)	Y^{2D}(N/m)	ν^{2D}	γ^{2D}(N/m)
Y_2CF_2	143.65	143.65	27.25	58.20	138.49	0.190	85.45
Y_2CCl_2	123.91	123.91	31.17	46.37	116.07	0.252	77.54
Y_2CBr_2	118.59	118.59	21.93	48.33	114.54	0.185	70.26
Y_2CI_2	120.04	120.04	29.52	45.26	112.78	0.246	74.78
Y_2CO_2	152.06	152.06	65.72	43.17	108.89	0.432	108.89

TOC Graphic